EXO-200 and the Search for Neutrinoless Double-Beta Decay

Tim Daniels, University of North Carolina Wilmington, on behalf of the EXO-200 Collaboration

Email: danielst@uncw.edu

Double-Beta Decay and Neutrino Physics

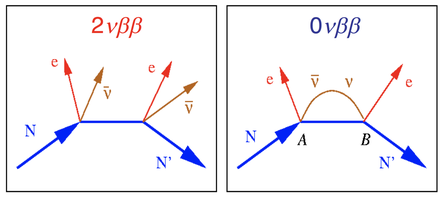

Figure 1: Left: Conventional $2\nu\beta\beta$ decay. Right: Exchange of a light Majorana neutrino is one possible mechanism for the hypothetical $0\nu\beta\beta$ mode.

Conventional two neutrino double-beta decay ($2\nu\beta\beta$) (Figure 1 left panel) has been observed in a range of nuclei for which single β-decay is forbidden. Observation of the hypothetical ($0\nu\beta\beta$) mode (Figure 1 right panel) would prove the existence of Majorana neutrinos, demonstrate lepton number non-conservation, and constrain the neutrino mass scale.

With limits on the $0\nu\beta\beta$ half-life at 10^{25} years, experimental searches must optimize isotopic abundance, energy resolution, radioactive backgrounds, and detection efficiency.

The EXO-200 Experiment

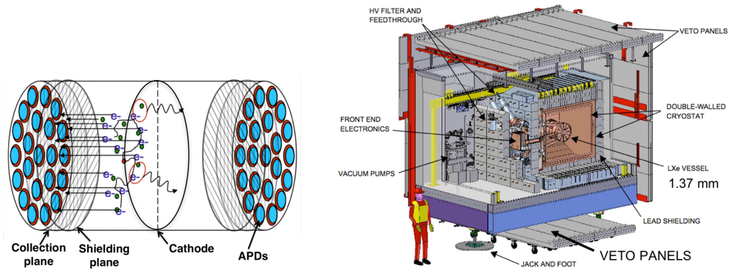

Figure 2: Left: TPC Diagram. Right: Detail of the underground cleanroom containing the detector and its surrounding cryostat.

The EXO-200 detector (Figure 2 left panel) is a liquid xenon time projection chamber (TPC). The ionization signal for each event is detected in one of two drift regions around a central cathode by crossed induction and collection wire grids, while the scintillation signal is detected by two avalanche photo-diodes (APD) arrays behind the wire grids.

The two signals are combined to measure the event energy. The TPC also determines a 3D position for each event, X/Y from the wire grids and Z from the time difference between the signals and the known drift velocity. Deposits spaced by about a cm or more can be resolved and assigned positions with an accuracy of a few mm.

Located at a depth of 1624 mwe in the Waste Isolation Pilot Plant (WIPP) outside Carlsbad, NM, the experiment (Figure 2 right panel) employs 110 kg of active xenon enriched to 80.6% in isotope 136. Data were collected in two phases between May 2011 and December 2018 for a total exposure of 234.1 kg-yr.

Background Discrimination

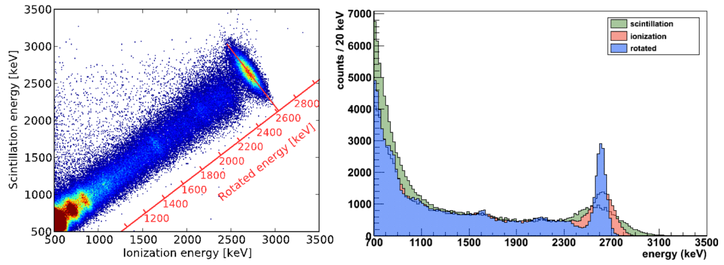

Figure 3: Left: 2D plot of scintillation energy and ionization energy from an external ^{228}Th calibration source. Right: 1D plots of the individual ionization and scintillation energies together with the optimized combination represented by the projection onto the "rotated" axis shown in the 2D plot.

Fluctuations in the ionization and scintillation signals are anticorrelated, as illustrated in the left panel of Figure 3. This is exploited in the combination of the the signals to improve the resolution of the energy measurement, as evident in the right panel. The average energy resolution (σ/E) at the ^{136}Xe $0\nu\beta\beta$ Q-value in Phase I was 1.35%, further improved to 1.15% in Phase II after an upgrade to the front-end electronics to address coherent noise in the scintillation readout.

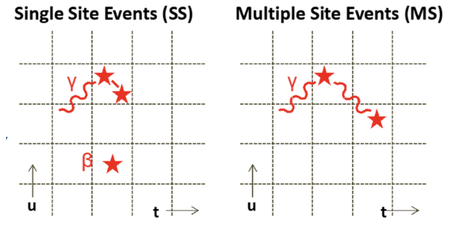

Figure 4: Illustration of the greater spatial extent typical of energy deposits from gamma-rays, which tend to Compton scatter at multiple locations, from those of localized beta decays.

The 3D event position provided by the TPC allows the experiment to exploit topological differences (see Figure 4) to discriminate energy deposits from beta decays from gamma-ray backgrounds. Events are sorted into "single site" (SS) or "multisite" (MS) spectra depending on the number of resolved energy deposits, with the former dominated by beta decays and the latter by gamma-ray events.

Further background discrimination within the SS and MS events is achieved by gleaning additional topological information directly from the signal waveforms with a deep neural network (DNN) $0\nu\beta\beta$ trained on simulated charge collection waveforms for beta and gamma decays. (Figure 5, left panel). This approach slightly outperformed a boosted decision tree (BDT) analysis formed around signal rise time, standoff distance, and number of channels.

External gamma-ray backgrounds sources can also be distinguished from internal beta decays by their attenuation in the liquid xenon as a function of "standoff distance" from the nearest detector component excluding the cathode (Figure 5, right panel).

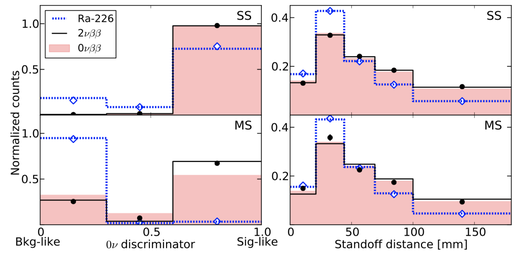

Figure 5: Comparison between data (dots) and simulation (lines) of the discriminator output (left) and standoff distance (right) for ^{226}Ra gamma-rays (blue), $2\nu\beta\beta$ decays (black), and simulated $0\nu\beta\beta$ decays (red). The difference between $0\nu\beta\beta$ and $2\nu\beta\beta$ events in the DNN in MS is due to the higher rate of bremsstrahlung at higher electron energy.

Results from the Complete Dataset

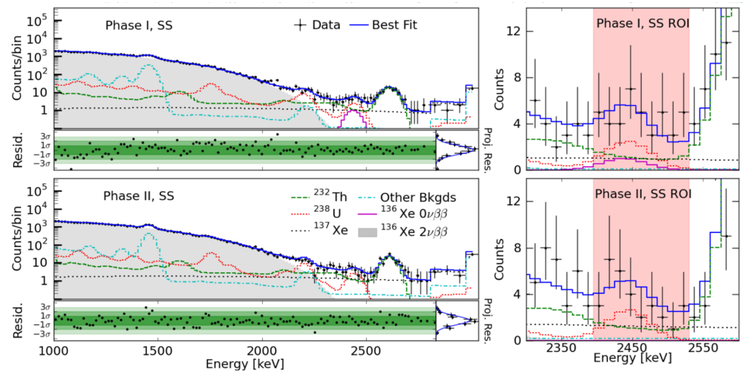

Figure 6: Best fit to the SS energy spectra for Phase I (top) and II (bottom). The righthand panels show zoomed-in views around the $0\nu\beta\beta$ Q-value.

SS and MS spectra are fit simultaneously for Phase I and Phase II data along three axes: event energy, standoff distance, and the DNN discriminator output. The fit for SS event energy is shown in Figure 6. The mean sensitivity to the ^{136}Xe $0\nu\beta\beta$ halflife is $5.0\text{x}10^{25}$ yr at the 90% confidence level. No statistically significant evidence for the decay is observed, and a lower limit of $3.5\text{x}10^{25}$ yr is set at the same confidence level. This results in upper limits on the Majorana neutrino mass of 78 - 239 meV for a range of nuclear matrix elements.

Further details: G. Anton *et al.*, *Phys. Rev. Lett.* 123, 161802 (2019).

Acknowledgements

EXO-200 is supported by DOE and NSF in the United States, NSERC in Canada, SNF in Switzerland, IBS in Korea, RFBR (18-02-00550) in Russia, DFG in Germany, and CAS and ISTCP in China. EXO-200 data analysis and simulation uses resources of the National Energy Research Scientific Computing Center (NERSC). We gratefully acknowledge the KARMEN collaboration for supplying the cosmic-ray veto detectors, and the WIPP for their hospitality.